Assessment of Proteins Associated With Complement Activation and Inflammation in Maculae of Human Donors Homozygous Risk at Chromosome 1 *CFH*-to-*F13B*

Tiarnan D. L. Keenan,[1,2] Marc Toso,[1] Chris Pappas,[1] Lisa Nichols,[1] Paul N. Bishop,[2] and Gregory S. Hageman[1]

[1]Center for Translational Medicine, John A. Moran Eye Center, Department of Ophthalmology and Visual Sciences, University of Utah, Salt Lake City, Utah, United States
[2]Centre for Ophthalmology & Vision Science, Institute of Human Development, Faculty of Medical and Human Sciences, University of Manchester and Manchester Royal Eye Hospital, Central Manchester University Hospitals NHS Foundation Trust, Manchester Academic Health Science Centre, Manchester, United Kingdom

Correspondence: Tiarnan D.L. Keenan, Institute of Human Development, AV Hill Building, University of Manchester, Oxford Road, Manchester M13 9PT, UK; tiarnan.keenan@doctors.org.uk.

Submitted: April 1, 2015
Accepted: June 22, 2015

Citation: Keenan TDL, Toso M, Pappas C, Nichols L, Bishop PN, Hageman GS. Assessment of proteins associated with complement activation and inflammation in maculae of human donors homozygous risk at chromosome 1 *CFH*-to-*F13B*. *Invest Ophthalmol Vis Sci*. 2015;56:4870–4879. DOI:10.1167/iovs.15-17009

Purpose. To determine the effects of chromosome 1 genotype and cigarette smoking on levels of complement activation and inflammation in the human macula.

Methods. Donor macular tissue was stratified into three groups by diplotype at the AMD-associated *CFH*-to-*F13B* locus: homozygous "risk" ($n = 9$, 56–78 years), homozygous neutral ($n = 2$, 64–79 years), and homozygous "protective" ($n = 6$, 61–78 years) diplotype. Importantly, all donors were homozygous nonrisk at the *ARMS2/HTRA1* locus, so that purely chromosome 1–directed pathways were examined. Immunohistochemistry was performed by using 14 antibodies, mostly against markers of complement and inflammation, followed by confocal microscopy and immunofluorescence quantification (all masked to donor status).

Results. Donors homozygous risk at *CFH*-to-*F13B* exhibited significantly higher levels of terminal complement complex (TCC) in macular Bruch's membrane (BM; $P = 0.03$), choriocapillaris (CC; $P = 0.04$), and choriocapillaris intercapillary septa (CC IS; $P = 0.03$), compared to homozygous protected donors. Smoking was associated with increased TCC in BM ($P = 0.05$), CC IS ($P = 0.03$), and choroidal stroma (CS; $P = 0.01$), and with substantially elevated C-reactive protein (CRP) levels in RPE ($P = 0.04$), BM ($P = 0.01$), CC ($P = 0.05$), and CS ($P = 0.05$). Smoking was associated with higher levels of oxidative stress in macular RPE ($P = 0.04$) and CS ($P = 0.01$).

Conclusions. Genetic risk at the *CFH*-to-*F13B* locus was associated with higher levels of complement activation at the human macular RPE–choroid interface, as was cigarette smoking. Levels of CRP were substantially elevated in risk donors with smoking history. Examination of human macular tissue from donors with "pure" diplotypes allows assessment of AMD-associated pathways driven solely by *CFH*-to-*F13B*. These findings have important implications for identifying chromosome 1–directed pathways and therapeutic targets.

Keywords: age-related macular degeneration, macula, immunohistochemistry, inflammation, complement factor H

Age-related macular degeneration (AMD) is the leading cause of blindness and visual impairment in developed countries.[1] It has major implications for society, as patients with AMD experience many years of reduced quality of life, loss of independence, and often depression.[2–4] Currently, there are no clinical treatments for atrophic AMD; existing drugs for neovascular AMD are palliative, and their efficacy is poor in many patients ("nonresponders").[5,6] To identify novel therapeutic targets for AMD, it is therefore necessary to refine our understanding of AMD pathogenesis and the molecular determinants of disease.

The genetic basis of AMD has largely been unraveled in recent years.[7–13] Strong associations have consistently been demonstrated with haplotypes at two major loci: (1) variants associated with genes (complement factor H [CFH], complement factor H–related 1-5, and factor 13B) at a locus on chromosome 1, which encode components and regulators of the complement system; and (2) variants associated with two tightly linked genes on chromosome 10q31 (*ARMS2/HTRA1*). Other genetic risk factors have also been identified by recent genome-wide association studies and continue to be reported,[7–12] but these genes exhibit only minor associations and account for a small percentage of patients with AMD.

Biochemical evidence has also strongly implicated complement dysregulation locally in the eye in disease pathogenesis.[14–16] Levels of the terminal complement complex (TCC, or C5b-9), the final common product of all complement activation pathways, are known to increase with age in macular RPE–choroid.[17,18] One previous report[19] has suggested that amounts of the TCC are higher in macular RPE–choroid from donors homozygous risk at the Y402H polymorphism in *CFH*.

Copyright 2015 The Association for Research in Vision and Ophthalmology, Inc.

Downloaded from iovs.arvojournals.org on 10/28/2021

However, previous research comparing macular tissue from AMD versus control donors has not always taken into account disease complexity based on genetic status. In particular, understanding of the genetic basis of AMD suggests that the disease may consist of at least two partially distinct entities[20,21]: one is caused by genetic variants in chromosome 1, where disease is driven predominantly by the complement system; individuals tend to develop large soft drusen in the macula over time, and are predisposed to geographic atrophy more than neovascular disease. By contrast, the other entity is caused by variants in chromosome 10; individuals generally develop fewer large macular drusen, and tend to progress to neovascular disease more than geographic atrophy.[22] This concept is demonstrated by the ability of AMD risk prediction models to discriminate between risk of atrophic and neovascular AMD.[23] For these reasons, it was deemed productive to study macular tissue from donors with "pure" genotypes, for example, AMD associated with risk variants at chromosome 1 without any additional risk at chromosome 10.

In addition to genetic variation and aging, environmental factors play an important role in AMD pathogenesis. In particular, cigarette smoking is strongly and consistently associated with disease, increasing risk by 2- to 4-fold.[24,25] Combined with other observations, this association suggests that oxidative stress plays an important role in AMD pathophysiology.[26,27] However, the exact mechanism whereby smoking increases AMD risk is unknown, and it is not clear how its effects may interact with genetic risk, for example, through interactions with the complement system.

In this study, we used immunohistochemistry on human macular tissue from donors with pure risk and nonrisk diplotypes to assess AMD-associated pathways that are driven solely by the *CFH*-to-*F13B* gene locus, and to examine the potential effects of cigarette smoking on these pathways.

Materials and Methods

Donor Eye Tissue

Postmortem human donor eyes were obtained from the Utah Lions Eye Bank (Salt Lake City, UT, USA). They were selected from 1601 donors with a date of death between May 2010 and May 2014. In all cases prior consent had been obtained for the ocular tissue to be used for research, and the research adhered to the tenets of the Declaration of Helsinki. The eyes were fixed in 4% (vol/vol) paraformaldehyde, within 4 hours post mortem, for 2 hours at 4°C, then stored in sodium cacodylate buffer at 4°C. Medical and ophthalmic histories (including information on tobacco/smoking history), a family questionnaire, blood, and sera were obtained from most donors (and all donors used in this study). Eyes were classified by using standardized fundal photography and AMD grading criteria, as previously described.[28]

AMD Genotyping

DNA was extracted from whole blood by using the QIAamp DNA Blood Maxi Kit (Qiagen, Valencia, CA, USA). Single nucleotide polymorphism (SNP) genotypes were then determined by using the TaqMan platform (Applied Biosystems [ABI], Waltham, MA, USA) under the manufacturer's recommended conditions. All SNP assays were predesigned with the exception of rs1061170, which was made by using ABI's Custom TaqMan Assay Design Tool. Samples were amplified by using a PTC-225 Thermal Cycler (Madison James Research, Asheboro, NC, USA) and analyzed on the Applied Biosystems 7900HT Fast Real-Time PCR System.

Selection of Donor Eyes for Immunohistochemistry

Donor eyes were selected and stratified into groups by diplotype at the AMD-associated *CFH*-to-*F13B* locus (Table 1), including homozygous risk diplotype, homozygous neutral diplotype, and homozygous protective diplotype. Importantly, all donors were homozygous nonrisk at the *ARMS2/HTRA1* locus on chromosome 10. Diplotype assignment was made on the basis of eight tagging SNPs within the *CFH*-to-*F13B* locus (Table 2), as previous research[23] has demonstrated that these provide the most parsimonious combination of SNPs for allocation of donors into five common haplotypes.

Age-related macular degeneration was not an inclusion or exclusion criterion and tissue selection was made blind to the presence or absence of AMD, either through positive clinical history or the presence of postmortem evidence of AMD before tissue sectioning. This information was revealed after image analysis and it transpired that none of the study donors had a clinical diagnosis of AMD or were found to have AMD by standardized grading of the postmortem tissue. Aside from AMD genotype, inclusion criteria for the donors were Caucasian race, age between 55 and 79 years (i.e., aiming for predominantly preclinical phase of disease; see Discussion), and a complete and verified medical and ophthalmic history. Donors were excluded from the study if they had a past history of glaucoma, diabetic retinopathy, retinal vascular occlusion, or retinal detachment. In addition, the presence of hepatic disease was used as an exclusion criterion, as this could influence CFH levels.

From genetic analyses of the 1601 donors, and applying the inclusion/exclusion criteria, 24 risk, 2 neutral, and 7 protective diplotype donors with no risk variants at *ARMS2/HTRA1* were identified. One randomly chosen donor from the risk and protective diplotype groups was kept back for other studies, leaving 23 risk, 2 neutral, and 6 protective diplotype donors. Of these, all of the neutral and protective diplotype donors were analyzed. The 23 risk diplotype donors were subdivided into smokers at time of death and nonsmokers/ex-smokers; four of the smokers and five of the nonsmokers/ex-smokers were chosen at random from these two groups for analysis.

Preparation of Macular Tissue for Immunofluorescence Microscopy

Immunohistochemistry, microscopy, and image analysis were performed under blinded conditions, that is, without knowledge of the age, genotype, or clinical history of the donor. Six-millimeter-diameter trephine-generated punches of the macula (RPE–choroid and retina), centered on the fovea, were obtained. The discs of macular tissue were embedded in 10% agarose (wt/vol, type XI, low-gelling temperature; Sigma-Aldrich Corp., St. Louis, MO, USA) at 45°C, and tissue sections of 100-μm thickness were made by using a Vibratome 1000 (Vibratome, St. Louis, MO, USA). After extensive washing with PBS, the tissue sections were blocked by incubation at room temperature for 6 hours with PBS containing 1 mg/mL BSA, 1% (vol/vol) goat serum, and 0.1% (vol/vol) Triton X-100. Immunohistochemistry was performed by using 14 antibodies against markers of oxidative stress, inflammation, complement regulation and activation, and other molecules of interest (Table 3). For each experiment, the relevant primary antibody was diluted in blocking buffer, applied to tissue sections (200 μL/section), and incubated for 16 hours at 4°C. After washing with PBT (PBS containing 1 mg/mL BSA and 0.1% [vol/vol] Triton X-100; three separate washes of 15 minutes duration each, at room temperature), tissue sections were incubated with fluorescently labeled secondary antibody (either Alexa-

Investigative Ophthalmology & Visual Science

Downloaded from iovs.arvojournals.org on 10/28/2021

Investigative Ophthalmology & Visual Science

TABLE 1. Details of Eyes Used in Immunohistochemical Analysis

Genotype Group	Donor Code	Age, y	Sex	Diplotype at *CFH*-to-*F13B*	Smoking History	Cause of Death	Ophthalmic History	Relevant Medical History	*C3* Genotype: rs2231099
Risk	0842-13 OD	56	M	H1-H2	Current	Sepsis	None	COPD	CC
	0454-11 OS	64	M	H1-H2	Current	Septic shock, respiratory failure	Bilateral cataract	COPD	CG
	0220-14 OD	64	M	H1-H2	Never	Respiratory failure	Left phaco + IOL	Parkinson's disease, multiple sclerosis	CC
	0678-12 OD	65	M	H1-H1	Ex-smoker	Aspiration pneumonia	Bilateral phaco + IOL	DM (no DR)	CC
	1566-12 OS	66	M	H1-H1	Ex-smoker	Respiratory failure, multiple organ failure	None	DM (no DR)	CC
	0276-13 OS	66	M	H2-H2	Current	Sepsis	None	COPD	CC
	1538-12 OD	67	M	H1-H2	Current	Pneumonia	None	None	CG
	0685-13 OS	72	F	H1-H1	Never	Endometrial cancer	OD retinal vascular occlusion	None	CC
	0260-11 OS	78	M	H1-H2	Never	Perioperative (aortic valve surgery)	Bilateral phaco + IOL	None	CC
Neutral	0346-12 OS	64	M	H4-H4	Current	Septic shock, respiratory failure	Left phaco + IOL	None	CC
	0736-12 OS	79	F	H4-H4	Never	Pancreatic cancer	Bilateral phaco + IOL	DM	CC
Protected	0715-11 OD	61	M	H3-H3	Never	Respiratory failure, colon cancer	None	DM (no DR)	CC
	0865-10 OS	65	M	H3-H3	Current	Respiratory failure, leukemia	Bilateral phaco + IOL	COPD, DM (no DR)	CC
	0300-11 OS	73	M	H3-H3	Current	Congestive cardiac failure	None	COPD, DM (no DR), dementia	CG
	0031-12 OS	76	F	H3-H3	Never	Myocardial infarction	Left phaco + IOL	DM (no DR)	CG
	0078-13 OD	77	M	H5-H5	Never	Chronic renal failure	Bilateral phaco + IOL	None	GG
	1168-13 OS	78	F	H5-H5	Ex-smoker	Myocardial infarction	None	Lung cancer	CG

CC, homozygous nonrisk; DM, diabetes mellitus; DR, diabetic retinopathy; GG, homozygous risk; phaco, phacoemulsification.

Fluor-488 goat anti-mouse IgG or AlexaFluor-488 goat anti-rabbit IgG, or AlexaFluor-488 goat anti-mouse IgM/IgG for 10E4; all from Invitrogen, Waltham, MA, USA), diluted 1:200 in PBT, for 16 hours at 4°C. After washing with PBT (three separate washes of 15 minutes' duration each, at room temperature), tissue sections were mounted on Superfrost microscope slides (Electron Microscopy Sciences, Hatfield, PA, USA) with Fluoro-Gel mounting medium (containing 4′,6-diamidino-2-phenylindole [DAPI] as a nuclear counterstain; Electron Microscopy Services). Microscope slides were stored at 4°C in the dark for 1 week before immunofluorescence imaging.

For experiments using the 3G10 antibody against heparan sulfate, tissue sections underwent enzymatic digestion with heparinase III from *Flavobacterium heparinum* (Amsbio, Cambridge, MA, USA), comprising 0.002 IU enzyme in 200 μL digestion buffer (0.1 M sodium acetate, 5 mM calcium chloride, pH 7.0) per tissue section, for 4 hours at 37°C, before blocking and antibody incubation steps. Control experiments were conducted where tissue sections were incubated with blocking buffer instead of primary antibody. Control experiments for procedures using the 3G10 antibody were conducted by incubation with digestion buffer without heparinase III, before staining. In all experiments, at least two tissue sections from the macular punch for each donor were stained for each antibody.

Image Capture and Data Analysis

Images were obtained by using a Fluoview 1000 laser scanning confocal microscope (Olympus America, Melville, NY, USA), using standardized methodology. In all cases, identical settings were used for image acquisition; the HV (sensitivity) setting had previously been optimized for each primary antibody and was maintained constant between all donors for each probe to ensure consistency. The confocal microscopy specifications were as follows: magnification ×20; AlexaFluor-488 laser intensity 6% (HV 350–400, predetermined for each antibody); DAPI laser intensity 4% (HV 400); 80-μm aperture; 20 μs/pixel; Kalman averaging (×2). For each tissue section examined, three images were obtained at random locations (approximately 1-mm diameter each), with the locations chosen under DAPI viewing conditions (as opposed to those for AlexaFluor-488). Since either two or three tissue sections were stained for each antibody for each donor, with three images obtained for each tissue section, a total of six or nine images were analyzed in each case.

Gray scale images of macular RPE–choroid and retina were analyzed by using ImageJ64 (v1.40g; http://imagej.nih.gov/ij/; provided in the public domain by the National Institutes of Health, Bethesda, MD, USA). For all antibodies (except where stated otherwise), staining was quantified in four anatomic areas of interest, specifically, the retinal pigment epithelium (RPE), Bruch's membrane (BM), choriocapillaris (CC), and choroidal stroma (CS). For the antibodies against TCC, C3/C3b, and vitronectin, staining was also quantified in the choriocapillaris intercapillary septa (CC IS), as these structures are labeled very clearly and intensely by these antibodies (see Figs. 1B, 1D, 1F, 2F). Finally, for antibodies against carboxymethyllysine (CML), 4-hydroxynonenal (HNE), membrane cofactor protein (MCP), and decay accelerating factor (DAF), staining was also quantified in the retina, as these markers of oxidative stress and cell-surface homologues of CFH are known from previous studies[29–31] to be present in the human neurosensory retina.

For each image, a polygon was drawn around the relevant anatomic structure, across the whole length of the tissue imaged (see Supplementary Fig. S1 for demonstration of segmentation

Downloaded from iovs.arvojournals.org on 10/28/2021

Table 2. Single Nucleotide Polymorphisms Used to Define *CFH*-to-*F13B* Haplotypes

Haplotype No.	AMD Risk or Protection	rs800292 (I62V)	rs1061170 (Y402H)	rs1410996	rs12144939*	rs7546940	rs1409153	rs10922153	rs698859
H1	Risk	G	C	G	G	G	C	G	C
H2	Risk	G	C	G	G	G	C	G	T
H3	Protection	A	T	A	G	G	T	T	C
H4	Neutral	G	T	G	G	A	T	T	T
H5	Protection	G	T	A	T	G	T	T	C

* Usually tags the *CFHR3/1* deletion.

into relevant anatomic areas), and ImageJ was used to calculate the mean fluorescence per unit area within the polygon. This process was repeated for all images, generating six or nine values of fluorescence for each anatomic area with each antibody for each donor, and the mean of these values was obtained. Similar analysis was performed on the images of the control/blank tissue sections. For each antibody on each donor, the mean blank signal was then subtracted from the mean test signal to generate the final representative value.

Primary statistical analysis was conducted by using the Mann-Whitney *U* test. Where primary statistical analysis identified a significant difference by genotype and/or smoking status, secondary statistical analysis by two-way analysis of variance (ANOVA) was also applied following logarithmic transformation of data to stabilize variance.[32]

Results

Immunohistochemical Results for Complement Pathway Components

Immunohistochemistry for complement activation products in human macular RPE–choroid tissue was performed and quantified for all donors, under masked conditions. Donors that were homozygous risk at the *CFH*-to-*F13B* locus exhibited significantly higher levels of the TCC in macular BM ($P = 0.03$), CC ($P = 0.04$), and CC IS ($P = 0.03$) than homozygous protected donors (Figs. 1A, 1B; see Supplementary Fig. S2A for accompanying negative control experiments). In the CS, staining levels were weak (particularly with increased distance from the CC) and nonsignificantly higher in risk donors ($P = 0.26$); negligible staining was observed in the RPE. The differences observed between risk and protected donors were noted despite the fact that the risk donor group was younger on average than the protected group (mean, 66 vs. 72 years), where levels of TCC in human BM/choroid are known to increase with age,[17,18] and contained fewer donors with genetic risk at *C3* (rs2231099; 2/9 vs. 4/6). The results were consistent for staining obtained with both Dako (Carpinteria, CA, USA) and Quidel (San Diego, CA, USA) antibodies against the TCC (Table 3), with similar staining patterns observed for both antibodies.

Moreover, the degree of staining for TCC was higher in those donors with positive smoking histories than in those without (Figs. 1C, 1D; and Supplementary Fig. S2B for negative controls). The level was significantly higher in BM ($P = 0.05$), CC IS ($P = 0.03$), and CS ($P = 0.01$) but did not meet statistical significance in CC ($P = 0.14$) by two-way ANOVA (undertaken as primary statistical analysis had already identified a significant difference by genotype). Again, this was despite the fact that the smoking group was younger on average than the nonsmoking group (mean, 66 vs. 72 years) and contained a similar proportion of donors with risk at *C3* (4/10 vs. 2/7).

Immunohistochemistry was also performed for the complement component and amplification product C3/C3b (using a monoclonal antibody that recognizes C3, C3b, iC3b, and C3dg). Donors homozygous risk at the *CFH*-to-*F13B* locus had higher levels of C3/C3b in macular BM ($P = 0.08$), CC ($P = 0.02$), and CC IS ($P = 0.007$), compared to homozygous protected donors (Figs. 1E, 1F; and Supplementary Fig. S2C for negative controls). No significant differences were observed according to smoking status in the BM ($P = 0.33$), CC ($P =$

Table 3. Details of Antibodies Used in Immunohistochemical Analysis

Target Molecule	Antibody Clone/Name	Species and Clonality	Source	Antibody Dilution
C3/C3b*	1H8	Mouse mAb	Cedarlane (Burlington, NC, USA)	1:100
CFI	A247	Mouse mAb	Quidel	1:200
CFP	A233	Mouse mAb	Quidel	1:200
CML	CML26	Mouse mAb	Abcam (Cambridge, MA, USA)	1:150
CRP	Y284	Rabbit mAb	Abcam	1:150
DAF (CD55)	IA10	Mouse mAb	BD Pharmingen (San Diego, CA, USA)	1:100
Heparanase-1	ab109696	Rabbit pAb	Abcam	1:200
HNE	HNEJ-2	Mouse mAb	Abcam	1:200
C5b-9 (TCC)	aE11	Mouse mAb	Dako	1:50
C5b-9 (TCC)	A239	Mouse mAb	Quidel	1:400
MCP (CD46)	H-294	Rabbit pAb	Santa Cruz (Dallas, TX, USA)	1:25
Vitronectin	BV2	Mouse mAb	EMD Millipore (Temecula, CA, USA)	1:50
Heparan sulfate	10E4	Mouse mAb	Amsbio	1:200
Heparan sulfate	3G10†	Mouse mAb	Amsbio	1:500

* Antibody also recognizes iC3b/C3dg.
† Antibody recognizes heparan sulfate after digestion by heparinase III.

Investigative Ophthalmology & Visual Science

Downloaded from iovs.arvojournals.org on 10/28/2021

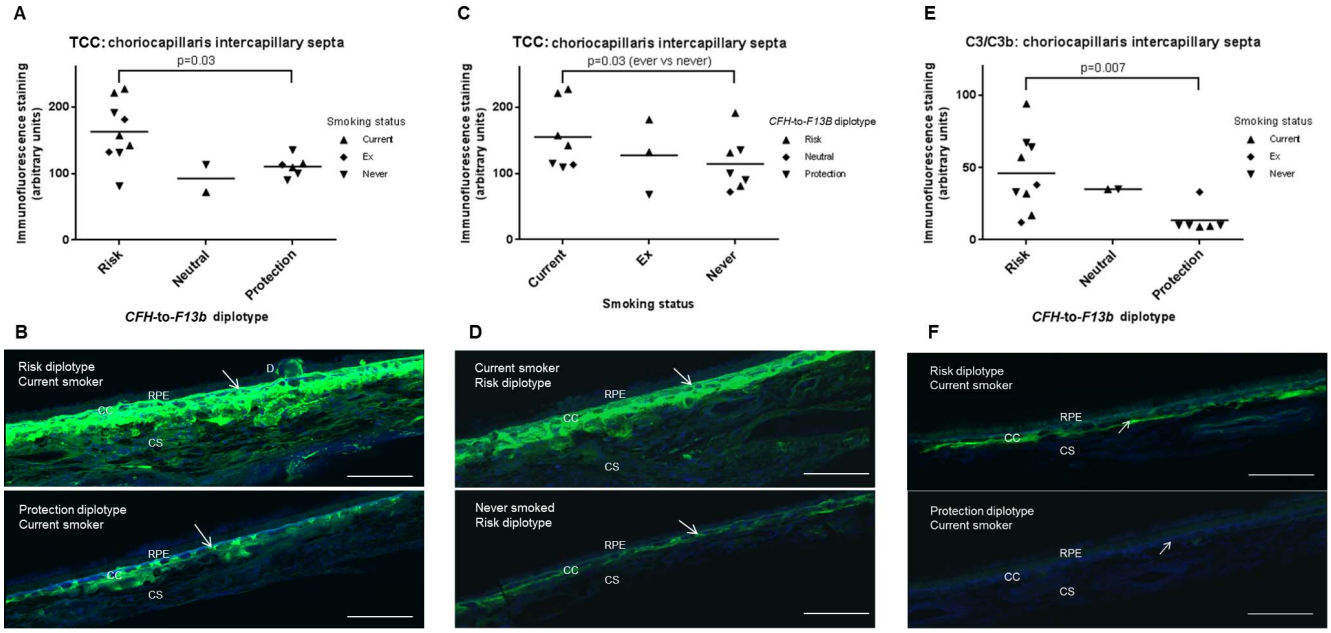

Figure 1. Immunolocalization/quantification of TCC and C3/C3b in human macular RPE–choroid tissue sections according to *CFH*-to-*F13B* diplotype and smoking status. (**A**) Quantification of TCC staining in CC IS; mean is shown, with value of statistical significance for risk versus protection diplotype, using Mann-Whitney *U* test ($P = 0.03$). (**B**) Immunolocalization of TCC using Quidel anti–C5b-9 monoclonal antibody (*green*) for two representative donors for *CFH*-to-*F13B* risk (0454-11 OS, 64-year-old male, current smoker) and protection (0300-11 OS, 73-year-old male, current smoker) diplotypes. (**C**) Quantification of TCC staining in CC IS; mean is shown, with value of statistical significance for ever versus never smoking status, using two-way ANOVA on log-transformed data ($P = 0.03$). (**D**) Immunolocalization of TCC using Quidel anti–C5b-9 monoclonal antibody (*green*) for two representative donors for positive smoking status (0454-11 OS, 64-year-old male, *CFH*-to-*F13B* risk diplotype) and negative smoking status (0260-11 OS, 78-year-old male, *CFH*-to-*F13B* risk diplotype). (**E**) Quantification of C3/C3b staining in CC IS; mean is shown, with value of statistical significance for risk versus protection diplotype, using Mann-Whitney *U* test ($P = 0.007$). (**F**) Immunolocalization of C3/C3b using anti–C3/C3b monoclonal antibody (*green*) for two representative donors for *CFH*-to-*F13B* risk (0276-13 OS, 66-year-old male, current smoker) and protection (0300-11 OS, 73-year-old male, current smoker) diplotypes. All images were processed in the same way. In all images, *blue* staining represents nuclear labeling by DAPI, and the *white scale bar* indicates 100 μm. The *white arrow* indicates CC IS. D, druse.

0.83), or CC IS ($P = 0.81$) by two-way ANOVA. Staining levels were extremely weak in the CS (i.e., labeling was confined for the most part to the CC, as observed previously[16]), and negligible in the RPE.

Complement factor I (CFI) is an important regulator of the complement system; in the alternative pathway, it cleaves and inactivates C3b (using CFH as a cofactor) to prevent excessive complement activation on host surfaces.[33] Complement factor I labeling was weakly present throughout the RPE, BM, CC, and CS, as observed in previous studies.[16] However, no significant differences were observed in the levels of CFI staining according to genotype or smoking, respectively, in the RPE ($P = 0.86$, $P = 0.31$), BM ($P = 0.16$, $P = 0.77$), CC ($P = 0.07$, $P = 0.22$), or CS ($P = 0.60$, $P = 0.53$). In addition, CFP (properdin) is the only known positive regulator of complement activation and can initiate complement activation through stabilization of the alternative pathway convertases.[34] Again, weak labeling of CFP was present throughout the RPE, BM, CC, and CS, but no significant differences were observed in levels of its staining according to genotype or smoking, respectively, in the RPE ($P = 0.41$, $P = 0.38$), BM ($P = 0.60$, $P = 0.38$), CC ($P = 0.77$, $P = 0.96$), or CS ($P = 0.73$, $P = 0.62$).

Membrane cofactor protein and DAF are cell-surface homologues of CFH and are able to regulate complement activation (in non–extracellular matrix environments).[35] Membrane cofactor protein labeling was present in the retina, RPE (abundant on its basal surface), CC, and CS, while DAF labeling was found in the retina, CC, and CS, but was very weak in the RPE, all as observed previously[16,31]; there was no significant staining of BM for either protein (as expected for this extracellular matrix). No significant differences were observed according to genotype in staining levels in macular retina or RPE–choroid for MCP (retina: $P = 0.73$, RPE: $P = 0.26$, CC: $P = 1.00$, CS: $P = 0.86$) or DAF (retina: $P = 0.52$, RPE: $P = 0.86$, CC: $P = 0.86$, CS: $P = 0.52$). Similarly, no differences were observed according to smoking status.

Immunohistochemical Results for C-Reactive Protein (CRP)

Labeling of the acute phase reactant CRP in macular tissue was generally moderate in the RPE and BM, and strong but variable between donors in the CC and CS (Fig. 2B), consistent with previous studies.[36,37] Indeed, donors with positive history of cigarette smoking had significantly higher levels of staining than those who had never smoked, in BM ($P = 0.05$) and CC ($P = 0.04$), but this did not meet statistical significance in the RPE ($P = 0.19$) or CS ($P = 0.06$) (Figs. 2A, 2B; and Supplementary Fig. S3A for negative controls). The difference was even more striking considering donors that continued smoking until death versus others: RPE ($P = 0.04$), BM ($P = 0.01$), CC ($P = 0.05$), and CS ($P = 0.05$).

Interestingly, no difference was observed in CRP levels, based on genotype in the RPE ($P = 0.86$), BM ($P = 0.95$), CC ($P = 0.73$), or CS ($P = 0.41$). However, qualitative analysis did strongly suggest that cigarette smoking was associated with very substantial elevation in CRP levels in the homozygous risk donors but not the protected donors (Figs. 2A, 2B). Indeed, two-way ANOVA (undertaken as primary statistical analysis had already demonstrated a significant difference by smoking

Investigative Ophthalmology & Visual Science

Downloaded from iovs.arvojournals.org on 10/28/2021

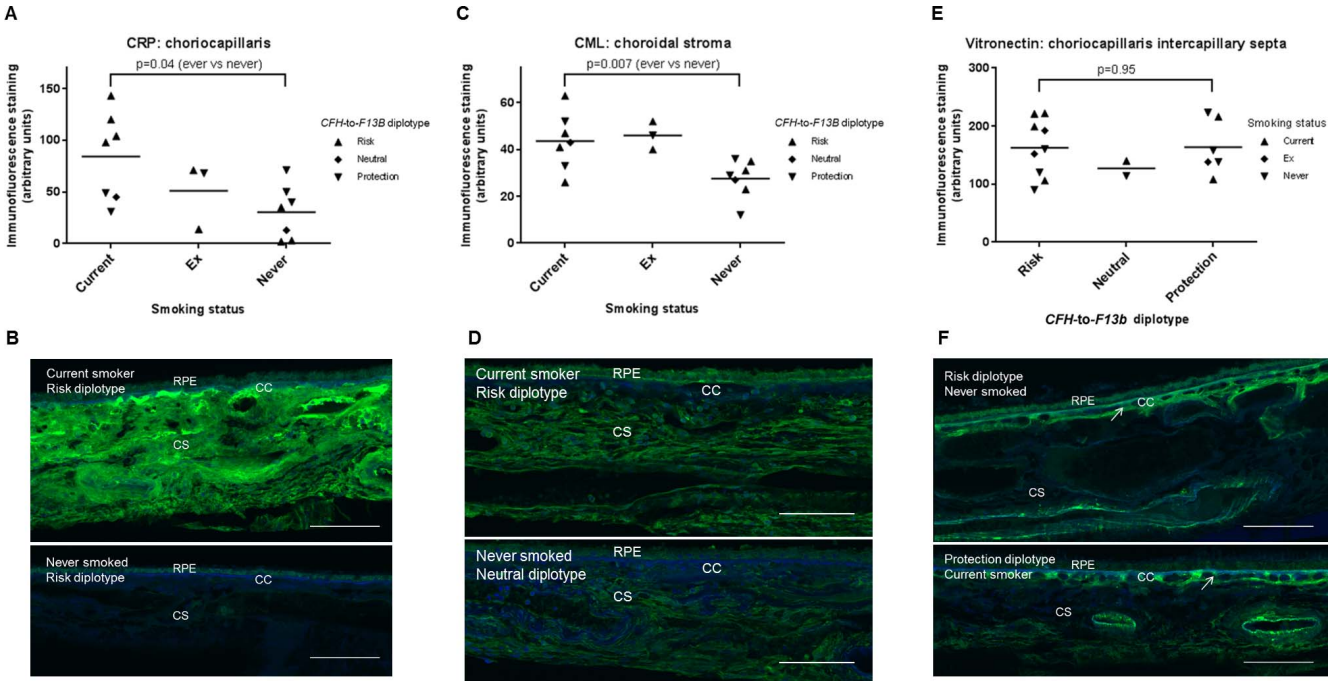

Figure 2. Immunolocalization/quantification of CRP, oxidative stress markers, and vitronectin in human macular RPE–choroid tissue sections according to smoking status and *CFH*-to-*F13B* diplotype. (**A**) Quantification of CRP staining in choriocapillaris; mean is shown, with value of statistical significance for ever versus never smoking status, using Mann-Whitney *U* test ($P = 0.04$). (**B**) Immunolocalization of CRP using anti-CRP monoclonal antibody (*green*) for two representative donors for positive smoking status (0842-13 OD, 56-year-old male, risk diplotype) and negative smoking status (0220-14 OD, 64-year-old male, risk diplotype). (**C**) Quantification of CML staining in CS; mean is shown, with value of statistical significance for ever versus never smoking status, using Mann-Whitney *U* test ($P = 0.007$). (**D**) Immunolocalization of CML using anti-CML monoclonal antibody (*green*) for two representative donors for positive smoking status (0454-11 OS, 64-year-old male, risk diplotype) and negative smoking status (0736-12 OS, 79-year-old female, neutral diplotype). (**E**) Quantification of vitronectin staining in CC IS; mean is shown, with value of statistical significance for risk versus protection diplotype, using Mann-Whitney *U* test ($P = 0.95$). (**F**) Immunolocalization of vitronectin using anti-vitronectin monoclonal antibody (*green*) for two representative donors for risk (0220-14 OD, 64-year-old male, never smoked) and protection (0300-11 OS, 73-year-old male, current smoker) diplotypes. All images were processed in the same way. In all images, *blue* staining represents nuclear labeling by DAPI, and the *white scale bars* indicate 100 μm. The *white arrow* indicates CC IS.

status) provided support for this idea; in CC, significance values for a positive effect were $P = 0.02$ (smoking), $P = 0.59$ (genetic risk), and $P = 0.025$ (interaction between smoking and genetic risk).

Immunohistochemical Results for Markers Associated With Oxidative Stress

The two biomarkers of oxidative stress used in this study were CML and HNE. Carboxymethyl-lysine is an advanced glycation end-product that is formed in tissues by nonenzymatic glycation and oxidation, and causes protein damage by cross-linking, changing tertiary structure, and altered enzymatic activity,[38] while HNE is a toxic product of lipid peroxidation that has been well characterized as a reliable marker of oxidative stress in tissues.[39] Labeling for both CML and HNE was observed consistently throughout the retina, RPE, BM, and choroid (Fig. 2D). However, donors with positive smoking history had higher levels of CML in the RPE ($P = 0.04$) and CS ($P = 0.007$; not quantified separately for CC) than those without, while no significant difference was observed in the BM ($P = 0.26$) (Figs. 2C, 2D; and Supplementary Fig. S3B for negative controls). For CML, no significant difference was observed according to genotype in the RPE ($P = 0.86$), BM ($P = 0.44$), or CS ($P = 0.47$). Staining levels for HNE were on average higher in donors with smoking history, but this tendency was not statistically significant in the RPE ($P = 0.31$), BM ($P = 0.38$), or CS ($P = 0.56$). As above, no difference was observed according to genotype in the RPE ($P = 0.77$), BM ($P = 0.29$), or CS ($P = 0.71$).

Immunohistochemical Results for Other Proteins of Interest

Vitronectin is a common component of the extracellular matrix and is abundantly present in drusen[40]; it can protect against complement-mediated damage, particularly through interactions with the TCC.[41] Labeling for vitronectin was particularly concentrated around the CC, including CC IS, and BM (see Fig. 2F), but was relatively weak in both the RPE and CS. No significant difference in levels of staining for vitronectin was observed according to *CFH*-to-*F13B* genotype or smoking, respectively, in macular RPE ($P = 0.95$, $P = 0.13$), BM ($P = 0.86$, $P = 0.53$), CC ($P = 0.48$, $P = 0.62$), CC IS ($P = 0.95$, $P = 0.70$), or CS ($P = 0.56$, $P = 0.38$) (Figs. 2E, 2F; and Supplementary Fig. S3C for negative controls).

Heparan sulfate is the major binding partner for CFH in human macular BM,[42,43] and the quantity of heparan sulfate in macular BM has been observed to decrease with age.[44] Heparan sulfate labeling (with either the 10E4 or 3G10 antibody) was present consistently throughout the retina, RPE, BM, CC, and CS layers, as we have observed in previous studies.[44,45] The level of staining with the 10E4 monoclonal antibody (which recognizes a common N-sulfated epitope in heparin sulfate[46]) did not differ according to genotype or smoking, respectively, in RPE ($P = 0.32$, $P = 0.19$), BM ($P = 0.64$, $P = 0.95$), CC ($P = 0.95$, $P = 0.95$), or CS ($P = 0.90$, $P =$

Investigative Ophthalmology & Visual Science

Downloaded from iovs.arvojournals.org on 10/28/2021

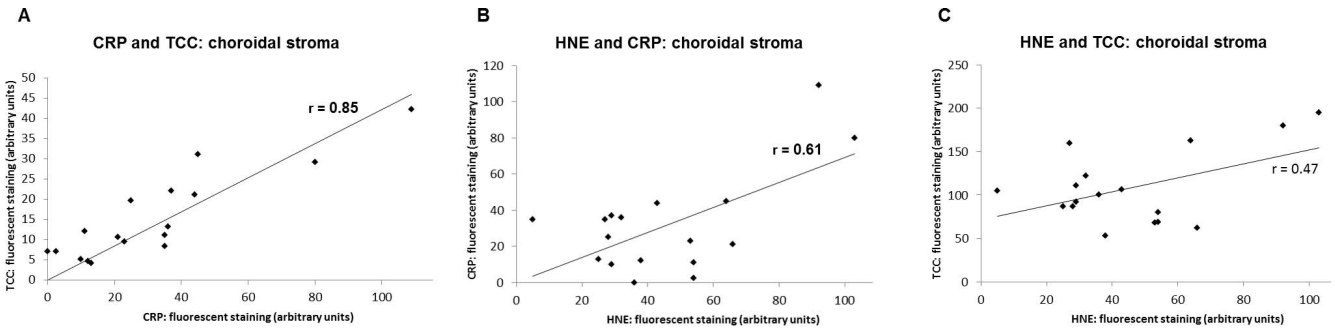

Figure 3. Analysis for potential correlation between levels of immunostaining for different markers in human macular RPE–choroid. (**A**) C-reactive protein and TCC in CS. (**B**) 4-Hydroxynonenal and CRP in CS. (**C**) 4-Hydroxynonenal and TCC in CS. In all graphs, the correlation coefficient *r* is given.

0.95). By contrast, the level of heparan sulfate staining with the 3G10 monoclonal antibody (which recognizes heparan sulfate stubs after digestion with heparinase III) did not differ by genotype in the RPE ($P = 0.60$) or BM (0.38), but was higher in risk donors in the CC ($P = 0.05$) and CS ($P = 0.02$); the level was also higher in current smokers than others in the RPE ($P = 0.03$), BM ($P = 0.03$), and CC ($P = 0.05$), but not the CS ($P = 0.59$).

Heparanase-1 is an important extracellular matrix enzyme that cleaves heparan sulfate chains in tissues and has been implicated in human disease including cancer, inflammation, and atherosclerosis.[47] Heparanase-1 labeling was found throughout the RPE, BM, and choroid, as we have observed previously.[44] However, no differences in levels of heparanase-1 staining were observed according to genotype in the RPE ($P = 0.48$), BM ($P = 0.64$), or CS ($P = 1.0$). While levels of staining were on average higher in donors with positive smoking history, these differences were not statistically significant in the RPE (0.07), BM ($P = 0.09$), or CS ($P = 0.10$).

Potential Correlation Between Immunohistochemical Results

In this analysis, immunohistochemical results in macular RPE–choroid were examined for potential correlations between different molecules of interest. The level of staining for CRP and the TCC showed strong–moderate correlation in BM ($r = 0.57$), CC ($r = 0.68$), and CS ($r = 0.85$) (Fig. 3A). In addition, markers of oxidative stress were analyzed against levels of CRP staining in CS and showed moderate correlation ($r = 0.61$ for HNE and $r = 0.51$ for CML; Fig. 3B). Finally, markers of oxidative stress were analyzed against levels of TCC staining in CS and showed moderate correlation ($r = 0.47$ for HNE and $r = 0.54$ for CML; Fig. 3C).

Discussion

In this study, we used human macular tissue from donors with pure *CFH*-to-*F13B* diplotypes in conjunction with a panel of antibodies to investigate potential molecular determinants of chromosome 1–directed AMD, specifically, markers of oxidative stress, complement activation, and inflammation. Importantly, all donors were homozygous nonrisk at the *ARMS2/HTRA1* locus on chromosome 10, in order that chromosome 1–directed pathways be assessed. Genetic risk at the *CFH*-to-*F13B* locus was associated with higher levels of complement activation at the RPE–choroid interface. Levels of complement activation were also higher in donors with history of cigarette smoking. In addition, cigarette smoking was associated with substantial elevations in levels of CRP in the macula, particularly in homozygous risk donors. Evidence was observed for increased levels of oxidative stress in the RPE–choroid of donors with positive smoking history. Finally, the observation of lower levels of C3/C3b in *CFH*-to-*F13B* protected donors supports the concept that donors with protective genotypes (specifically the I62V polymorphism and the *CFHR3/1* deletion) may be relatively protected against the development of AMD specifically through enhanced CFH-mediated complement regulation.

The strengths of this study includes the use of human donor macular tissue from a very large well-characterized eye repository that includes extensive genetic and clinical information on donor tissue. This enabled us to select donors with pure *CFH*-to-*F13B* diplotypes and without risk variants at the *ARMS2/HTRA1* locus. This approach is critical for identifying the molecular determinants of chromosome 1–directed AMD, as distinct from disease driven by chromosome 10. In addition, it enabled us to select donors from similar age groups; ages of 55 to 79 years were chosen for this study in order to identify altered levels of relevant proteins in the predominantly preclinical phase of disease, that is, before macular destruction through the extensive inflammation, atrophy, and/or choroidal neovascularization and scarring processes that may accompany advanced AMD. Indeed, no donors used in this study had AMD diagnosed clinically before death or on fundal photography of postmortem tissue. Further strengths of the study included the ability to select donors with verified positive and negative histories of cigarette smoking in both genetic groups.

Macular tissue from donors with pure diplotypes and uniformly short postmortem times was used in conjunction with a panel of well-characterized antibodies, much larger than numbers used in many previous studies, and including diverse markers involved in oxidative stress, complement activation, regulation, and inflammation (processes considered central to chromosome 1–directed AMD pathogenesis[14,16]). Most of these antibodies have been used and validated in previous immunohistochemical studies of ocular tissue,[16,17,36,44,45,48–50] and more than one antibody was used in some cases (e.g., for the TCC and for heparan sulfate). The entire study, from immunohistochemistry to microscopy and image analysis, was performed blinded to donor genotype and clinical status, and under standardized conditions, ensuring maximum confidence in any observed differences between groups. This clearly revealed that *CFH*-to-*F13B* genotype, together with smoking status, are major variables in determining levels of complement activation at the human macular RPE–choroid interface. Hence, a clear link was demonstrated between known epidemiologic risk factors for AMD and molecular pathology at the anatomic site of AMD formation.

Investigative Ophthalmology & Visual Science

Downloaded from iovs.arvojournals.org on 10/28/2021

The main limitation of the study was relatively modest sample size. When the genotype of 1601 donors was analyzed, donors with pure *CFH*-to-*F13B* diplotypes and without risk variants at the *ARMS2/HTRA1* locus were found to be rare, so the sample size was small. For similar reasons, it was not possible to age-match the groups closely, though we did find increased complement activation in homozygous risk donors despite this group being younger on average than the protected group. We also acknowledge that immunofluorescence is semiquantitative, that is, fluorescence intensity is not always proportional to the amount of antigen, though all staining and imaging protocols were performed in a standardized manner with identical settings. For this reason, and because of the relatively small sample size, primary statistical analysis was performed by using nonparametric testing (by Mann-Whitney *U* test). Where primary statistical analysis identified a significant difference by genotype and/or smoking status, secondary statistical analysis was undertaken by using parametric testing (by two-way ANOVA). Uncertainty over the normal distribution of these data means that the ANOVA results should be interpreted cautiously, though data were log-transformed to stabilize variance before testing.[32]

Several previous studies[17–19,51] have reported the presence of TCC in the Bruch's membrane/choriocapillaris complex, based on immunolocalization studies. However, there is no good evidence that any known antibodies can distinguish between the different forms of the TCC.[52] Terminal complement complex (C5b-9) can occur as a soluble form (SC5b-9), which binds vitronectin and is nonlytic, or as a membrane-bound form, which can recruit more C9 to form the lytic membrane attack complex (MAC). Therefore, the presence of extracellular TCC in Bruch's membrane and extracellular components of the choriocapillaris could indicate local production of SC5b-9 and therefore, local complement activation, MAC that has blebbed off cell membranes, or deposition of blood-borne SC5b-9. The reported relative concentration in the macular region does however favor the case for local formation of TCC.[51,53]

One previous study has reported increased levels of the TCC in the RPE–choroid of donors homozygous risk at the Y402H polymorphism in *CFH* by ELISA ($P = 0.04$; $n = 8$ for high risk and $n = 10$ for low risk),[19] in juxtamacular tissue, though other important donor variables are not reported in the article, including age, genetic risk at *C3* and *ARMS2/HTRA1*, and smoking status. A recent article by the same group[18] reports that levels of the TCC increase significantly with age, with AMD, and with risk at CFH_{Y402H}, but the study does not analyze TCC levels by *CFH*-to-*F13B* genotype in the absence of risk at the *ARMS2/HTRA1* locus. This is important, as AMD may comprise at least two partially distinct disease entities, one driven predominantly by risk at chromosome 1 and the other by risk at chromosome 10. For a refined understanding of potentially separate biological pathways involved, it is therefore essential to distinguish between AMD caused by variants at either locus. Indeed, this is the first study (to our knowledge) that performed immunolocalization of complement activation products and inflammatory markers in human macular tissue on a set of donors with pure *CFH*-to-*F13B* diplotypes, no risk at *ARMS2/HTRA1*, together with detailed smoking history. Despite the modest sample size presented here, this approach may be extremely fruitful in elucidating the precise pathobiology underpinning AMD driven by *CFH*-to-*F13B* genotype versus *ARMS2/HTRA1*.

Two previous studies have examined the level of CRP in human macular tissue, one according to CFH_{Y402H} genotype[36] and one according to AMD status.[37] Johnson et al.[36] have reported that *CFH* homozygote risk donors have significantly higher levels of CRP in the choroid by immunohistochemistry than homozygote nonrisk donors ($n = 6$ and $n = 9$, respectively). However, the smoking status of these donors is not reported; given the small sample size of the risk donors ($n = 6$), it is possible that CRP levels may have been elevated in donors through a combination of positive smoking history and *CFH* risk, rather than through the *CFH* risk alone. Bhutto et al.[37] have performed macular immunohistochemistry for CRP on 18 donors with AMD and 10 aged controls, and they have observed that staining intensity is significantly higher in AMD donors. Only three of the 18 donors were labeled as having positive smoking history; this proportion seems low for this age group, suggesting that accurate smoking history may not have been available. Indeed, many donors in the AMD group were labeled as having chronic obstructive pulmonary disease (COPD; usually caused by cigarette smoking; 4/8 in the early AMD group and 3/6 in the geographic atrophy group), which raises the possibility that smoking status (alone or in combination with *CFH* genetic risk) rather than AMD is the primary associate of raised CRP levels.

Other molecules were examined in this study owing to existing interest in their potential involvement in AMD pathogenesis, including markers of oxidative stress, heparan sulfate, and complement regulators such as CFI and vitronectin. Evidence for elevated levels of macular oxidative stress with cigarette smoking was observed, together with some correlation between levels of oxidative stress and complement activation; this supports the idea that oxidative stress is strongly implicated in AMD pathogenesis.[26,54] Heparan sulfate is the main binding partner for CFH in human macular BM[42,43]; its levels in this extracellular matrix have recently been shown to decrease with age, potentially leading to reduced quantities of CFH available to prevent complement activation.[44] Genotype was not found to alter levels of heparan sulfate in BM (though 3G10 labeling was higher in CC and CS with the risk diplotype). However, the level of 3G10 but not 10E4 staining in the RPE–choroid was higher in smokers. 3G10 recognizes heparan sulfate stubs after bacterial heparinase III digestion, so this result suggests that there are more heparan sulfate chains in smokers, while the overall amount of heparan sulfate (as assessed using the 10E4 antibody) was not different between smokers and nonsmokers. A possible explanation is that smoking results in heparan sulfate chain degradation, and to compensate there is increased heparan sulfate proteoglycan synthesis.

Overall, these findings enhance our understanding of AMD pathogenesis, specifically the pathobiology of chromosome 1–directed AMD. The findings that *CFH*-to-*F13B* risk and cigarette smoking are both associated with increased complement activation in macular RPE–choroid supports the hypothesis that local complement dysregulation is central to this form of AMD. It also suggests that therapeutic strategies to inhibit complement activation locally in the eye may be effective for individuals with chromosome 1–driven disease, though patients with mixed disease (i.e., driven by chromosome 10 also) may require different therapeutic strategies. Similarly, the close correlation between levels of complement activation and the inflammatory marker CRP reinforces the idea that complement dysregulation and chronic local inflammation are intimately related at the macular RPE–choroid interface in early AMD.

In conclusion, genetic risk at the *CFH*-to-*F13B* locus (in the absence of risk at the *ARMS2/HTRA1* locus) was associated with higher levels of complement activation at the human macular RPE–choroid interface, as was history of cigarette smoking. Levels of inflammation were substantially elevated in *CFH*-to-*F13B* risk donors with history of cigarette smoking, which was also associated with increased oxidative stress in all donors. Examination of human macular tissue from donors with "pure" diplotypes allows assessment of AMD-associated

Investigative Ophthalmology & Visual Science

Downloaded from iovs.arvojournals.org on 10/28/2021

pathways that are driven solely by the *CFH*-to-*F13B* gene locus. These findings have important implications related to the identification of chromosome 1–directed pathways and therapeutic targets.

Acknowledgments

We gratefully acknowledge the assistance of Anthony Day, PhD (Wellcome Trust Centre for Cell-Matrix Research, Faculty of Life Sciences, University of Manchester), with pilot studies related to this work. We also acknowledge the valuable contributions of Debra Schaumberg, MPH (Center for Translational Medicine, John A. Moran Eye Center, Department of Ophthalmology and Visual Sciences, University of Utah), and Andrew Dowsey, DPhil (Centre for Advanced Discovery and Experimental Therapeutics [CADET], University of Manchester and Central Manchester University Hospitals NHS Foundation Trust, Manchester Academic Health Science Centre, Manchester), for advice with statistical analysis.

Supported by the Fulbright/Fight for Sight UK-US Scholarship 2013/14 (TDLK).

Disclosure: **T.D.L. Keenan**, None; **M. Toso**, None; **C. Pappas**, None; **L. Nichols**, None; **P.N. Bishop**, None; **G.S. Hageman**, Allergan, Inc. (F), Ophtherion, Inc. (I), Voyant Biotherapeutics (I), AGTC (C), Gerson Lehrman (C), Novartis Pharmaceuticals (C), Sequenom, Inc. (C), P

References

1. Congdon N, O'Colmain B, Klaver CC, et al. Causes and prevalence of visual impairment among adults in the United States. *Arch Ophthalmol*. 2004;122:477–485.
2. Coleman AL, Yu F, Ensrud KE, et al. Impact of age-related macular degeneration on vision-specific quality of life: follow-up from the 10-year and 15-year visits of the Study of Osteoporotic Fractures. *Am J Ophthalmol*. 2010;150:683–691.
3. Bonastre J, Le Pen C, Anderson P, et al. The epidemiology, economics and quality of life burden of age-related macular degeneration in France, Germany, Italy and the United Kingdom. *Eur J Health Econ*. 2002;3:94–102.
4. Popescu ML, Boisjoly H, Schmaltz H, et al. Explaining the relationship between three eye diseases and depressive symptoms in older adults. *Invest Ophthalmol Vis Sci*. 2012; 53:2308–2313.
5. Kloeckener-Gruissem B, Barthelmes D, Labs S, et al. Genetic association with response to intravitreal ranibizumab in patients with neovascular AMD. *Invest Ophthalmol Vis Sci*. 2011;52:4694–4702.
6. Brown DM, Michels M, Kaiser PK, et al. Ranibizumab versus verteporfin photodynamic therapy for neovascular age-related macular degeneration: two-year results of the ANCHOR study. *Ophthalmology*. 2009;116:57–65.e5.
7. Chen W, Stambolian D, Edwards AO, et al. Genetic variants near TIMP3 and high-density lipoprotein-associated loci influence susceptibility to age-related macular degeneration. *Proc Natl Acad Sci U S A*. 2010;107:7401–7406.
8. Neale BM, Fagerness J, Reynolds R, et al. Genome-wide association study of advanced age-related macular degeneration identifies a role of the hepatic lipase gene (LIPC). *Proc Natl Acad Sci U S A*. 2010;107:7395–7400.
9. Yu Y, Bhangale TR, Fagerness J, et al. Common variants near FRK/COL10A1 and VEGFA are associated with advanced age-related macular degeneration. *Hum Mol Genet*. 2011;20: 3699–3709.
10. Cipriani V, Leung HT, Plagnol V, et al. Genome-wide association study of age-related macular degeneration identifies associated variants in the TNXB-FKBPL-NOTCH4 region of chromosome 6p21.3. *Hum Mol Genet*. 2012;21:4138–4150.
11. Fritsche LG, Chen W, Schu M, et al. Seven new loci associated with age-related macular degeneration. *Nat Genet*. 2013;45: 433–439.
12. Fritsche LG, Fariss RN, Stambolian D, et al. Age-related macular degeneration: genetics and biology coming together. *Annu Rev Genomics Hum Genet*. 2014;15:151–171.
13. Schramm EC, Clark SJ, Triebwasser MP, et al. Genetic variants in the complement system predisposing to age-related macular degeneration: a review. *Mol Immunol*. 2014;61:118–125.
14. Hageman GS, Luthert PJ, Victor Chong NH, et al. An integrated hypothesis that considers drusen as biomarkers of immune-mediated processes at the RPE-Bruch's membrane interface in aging and age-related macular degeneration. *Prog Retin Eye Res*. 2001;20:705–732.
15. Anderson DH, Mullins RF, Hageman GS, Johnson LV. A role for local inflammation in the formation of drusen in the aging eye. *Am J Ophthalmol*. 2002;134:411–431.
16. Anderson DH, Radeke MJ, Gallo NB, et al. The pivotal role of the complement system in aging and age-related macular degeneration: hypothesis re-visited. *Prog Retin Eye Res*. 2010; 29:95–112.
17. Seth A, Cui J, To E, Kwee M, Matsubara J. Complement-associated deposits in the human retina. *Invest Ophthalmol Vis Sci*. 2008;49:743–750.
18. Mullins RF, Schoo DP, Sohn EH, et al. The membrane attack complex in aging human choriocapillaris: relationship to macular degeneration and choroidal thinning. *Am J Pathol*. 2014;184:3142–3153.
19. Mullins RF, Dewald AD, Streb LM, et al. Elevated membrane attack complex in human choroid with high risk complement factor H genotypes. *Exp Eye Res*. 2011;93:565–567.
20. DeWan A, Bracken MB, Hoh J. Two genetic pathways for age-related macular degeneration. *Curr Opin Genet Dev*. 2007;17: 228–233.
21. Sobrin L, Reynolds R, Yu Y, et al. ARMS2/HTRA1 locus can confer differential susceptibility to the advanced subtypes of age-related macular degeneration. *Am J Ophthalmol*. 2011; 151:345–352.e3.
22. Chong EW, Amirul Islam FM, Robman LD, et al. Age-related macular degeneration phenotypes associated with mutually exclusive homozygous risk variants in cfh and htra1 genes. *Retina*. 2015;35:989–998.
23. Perlee LT, Bansal AT, Gehrs K, et al. Inclusion of genotype with fundus phenotype improves accuracy of predicting choroidal neovascularization and geographic atrophy. *Ophthalmology*. 2013;120:1880–1892.
24. Chakravarthy U, Wong TY, Fletcher A, et al. Clinical risk factors for age-related macular degeneration: a systematic review and meta-analysis. *BMC Ophthalmol*. 2010;10:31.
25. Woodell A, Rohrer B. A mechanistic review of cigarette smoke and age-related macular degeneration. *Adv Exp Med Biol*. 2014;801:301–307.
26. Khandhadia S, Lotery A. Oxidation and age-related macular degeneration: insights from molecular biology. *Expert Rev Mol Med*. 2010;12:e34.
27. Galor A, Lee DJ. Effects of smoking on ocular health. *Curr Opin Ophthalmol*. 2011;22:477–482.
28. Ferris FL III, Wilkinson CP, Bird A, et al. Clinical classification of age-related macular degeneration. *Ophthalmology*. 2013; 120:844–851.
29. Pawlak AM, Glenn JV, Beattie JR, McGarvey JJ, Stitt AW. Advanced glycation as a basis for understanding retinal aging and noninvasive risk prediction. *Ann NY Acad Sci*. 2008;1126: 59–65.
30. Ethen CM, Reilly C, Feng X, Olsen TW, Ferrington DA. Age-related macular degeneration and retinal protein modification

Investigative Ophthalmology & Visual Science

Downloaded from iovs.arvojournals.org on 10/28/2021

by 4-hydroxy-2-nonenal. *Invest Ophthalmol Vis Sci*. 2007;48:3469–3479.

31. Fett AL, Hermann MM, Muether PS, Kirchhof B, Fauser S. Immunohistochemical localization of complement regulatory proteins in the human retina. *Histol Histopathol*. 2012;27:357–364.
32. Feng C, Wang H, Lu N, Tu XM. Log transformation: application and interpretation in biomedical research. *Stat Med*. 2013;32:230–239.
33. Harrison RA, Lachmann PJ. The physiological breakdown of the third component of human complement. *Mol Immunol*. 1980;17:9–20.
34. Lesher AM, Nilsson B, Song WC. Properdin in complement activation and tissue injury. *Mol Immunol*. 2013;56:191–198.
35. Kim DD, Song WC. Membrane complement regulatory proteins. *Clin Immunol*. 2006;118:127–136.
36. Johnson PT, Betts KE, Radeke MJ, et al. Individuals homozygous for the age-related macular degeneration risk-conferring variant of complement factor H have elevated levels of CRP in the choroid. *Proc Natl Acad Sci U S A*. 2006;103:17456–17461.
37. Bhutto IA, Baba T, Merges C, et al. C-reactive protein and complement factor H in aged human eyes and eyes with age-related macular degeneration. *Br J Ophthalmol*. 2011;95:1323–1330.
38. Chen M, Curtis TM, Stitt AW. Advanced glycation end products and diabetic retinopathy. *Curr Med Chem*. 2013;20:3234–3240.
39. Shoeb M, Ansari NH, Srivastava SK, Ramana KV. 4-Hydroxynonenal in the pathogenesis and progression of human diseases. *Curr Med Chem*. 2014;21:230–237.
40. Hageman GS, Mullins RF, Russell SR, Johnson LV, Anderson DH. Vitronectin is a constituent of ocular drusen and the vitronectin gene is expressed in human retinal pigmented epithelial cells. *FASEB J*. 1999;13:477–484.
41. Singh B, Su YC, Riesbeck K. Vitronectin in bacterial pathogenesis: a host protein used in complement escape and cellular invasion. *Mol Microbiol*. 2010;78:545–560.
42. Clark SJ, Perveen R, Hakobyan S, et al. Impaired binding of the age-related macular degeneration-associated complement factor H 402H allotype to Bruch's membrane in human retina. *J Biol Chem*. 2010;285:30192–30202.
43. Clark SJ, Bishop PN, Day AJ. Complement factor H and age-related macular degeneration: the role of glycosaminoglycan recognition in disease pathology. *Biochem Soc Trans*. 2010;38:1342–1348.
44. Keenan TD, Pickford CE, Holley RJ, et al. Age-dependent changes in heparan sulfate in human Bruch's membrane: implications for age-related macular degeneration. *Invest Ophthalmol Vis Sci*. 2014;55:5370–5379.
45. Clark SJ, Keenan TD, Fielder HL, et al. Mapping the differential distribution of glycosaminoglycans in the adult human retina, choroid, and sclera. *Invest Ophthalmol Vis Sci*. 2011;52:6511–6521.
46. David G, Bai XM, Van der Schueren B, Cassiman JJ, Van den Berghe H. Developmental changes in heparan sulfate expression: in situ detection with mAbs. *J Cell Biol*. 1992;119:961–975.
47. Goldberg R, Meirovitz A, Hirshoren N, et al. Versatile role of heparanase in inflammation. *Matrix Biol*. 2013;32:234–240.
48. Johnson LV, Ozaki S, Staples MK, Erickson PA, Anderson DH. A potential role for immune complex pathogenesis in drusen formation. *Exp Eye Res*. 2000;70:441–449.
49. Vogt SD, Barnum SR, Curcio CA, Read RW. Distribution of complement anaphylatoxin receptors and membrane-bound regulators in normal human retina. *Exp Eye Res*. 2006;83:834–840.
50. Mullins RF, Russell SR, Anderson DH, Hageman GS. Drusen associated with aging and age-related macular degeneration contain proteins common to extracellular deposits associated with atherosclerosis, elastosis, amyloidosis, and dense deposit disease. *FASEB J*. 2000;14:835–846.
51. Hageman GS, Anderson DH, Johnson LV, et al. A common haplotype in the complement regulatory gene factor H (HF1/CFH) predisposes individuals to age-related macular degeneration. *Proc Natl Acad Sci U S A*. 2005;102:7227–7232.
52. Wurzner R. Immunohistochemical measurement of complement components and activation products. In: Morgan BP, ed. *Complement Methods and Protocols*. Totowa, NJ: Humana Press, Inc; 2000:103–112.
53. Mollnes TE, Lea T, Harboe M, Tschopp J. Monoclonal antibodies recognizing a neoantigen of poly(C9) detect the human terminal complement complex in tissue and plasma. *Scand J Immunol*. 1985;22:183–195.
54. Jarrett SG, Boulton ME. Consequences of oxidative stress in age-related macular degeneration. *Mol Aspects Med*. 2012;33:399–417.

Investigative Ophthalmology & Visual Science

Downloaded from iovs.arvojournals.org on 10/28/2021